Paleoceanography and Paleoclimatology

RESEARCH ARTICLE
10.1029/2019PA003606

Transport Bias by Ocean Currents in Sedimentary Microplankton Assemblages: Implications for Paleoceanographic Reconstructions

Peter D. Nooteboom[1,2], Peter K. Bijl[3], Erik van Sebille[1,2], Anna S. von der Heydt[1,2], and Henk A. Dijkstra[1,2]

[1]Institute for Marine and Atmospheric research Utrecht (IMAU), Department of Physics, Utrecht University, Utrecht, Netherlands, [2]Centre for Complex Systems Studies, Utrecht University, Utrecht, Netherlands, [3]Marine Palynology and Paleoceanography, Laboratory of Palaeobotany and Palynology, Department of Earth Sciences, Utrecht University, Utrecht, Netherlands

Key Points:
- We simulate the lateral transport of sinking dinoflagellate cysts in the modern ocean
- The transport from encystment to deposition influences the oceanographic signals preserved in sedimentary dinoflagellate cyst assemblages
- Accounting for systematic cyst transport could improve paleoceanographic inferrences from sedimentary microplankton distributions

Supporting Information:
- Supporting Information S1
- Supporting Information S2
- Figure S1
- Figure S2
- Figure S3
- Figure S4
- Figure S5
- Figure S6
- Figure S7
- Figure S8
- Figure S9
- Movie S1

Correspondence to:
P. D. Nooteboom,
p.d.nooteboom@uu.nl

Citation:
Nooteboom P. D., Bijl, P. K., van Sebille, E., von der Heydt, A. S., & Dijkstra, H. A. (2019). Transport bias by ocean currents in sedimentary microplankton assemblages: Implications for paleoceanographic reconstructions. *Paleoceanography and Paleoclimatology*, *34*, 1178–1194. https://doi.org/10.1029/2019PA003606

Received 21 MAR 2019
Accepted 14 JUN 2019
Accepted article online 19 JUN 2019
Published online 25 JUL 2019

Abstract Microfossils from plankton are used for paleoceanographic reconstructions. An often-made assumption in quantitative microplankton-based paleoceanographic reconstructions is that sedimentary assemblages represent conditions of the directly overlying surface water. However, any immobile particle sinking down the water column is subjected to transport by three-dimensional currents, which results in a lateral relocation along transport. We model dinoflagellate cyst (dinocyst) transport in a high-resolution (0.1° horizontally) global model of the present-day ocean and compare ocean conditions in the simulated origin of sedimentary particles to that in the directly overlying water. We find that the assumption that sedimentary particles represent the overlying surface waters is in most regions not valid. The bias induced by dinocyst transport depends on ocean current strength and direction, aggregation of particles which could increase the sinking speed, and the sediment sample depth. By using realistic sinking speeds of dinocysts and aggregates, extreme biases up to approximately ±16 °C warmer or ±4 PSU saltier are found, while other regions show lower bias from particle transport. Our model results provide a way to mechanistically and statistically explain the unexpected occurrences of some dinocyst species outside of their "normal" occurrence region, such as the northerly occurrence of the allegedly sea-ice-affiliated dinocyst *Selenopemphix antarctica*. Exclusion of such outlier occurrences will yield better constrained ecological affinites for dinocyst species, which has implications for microfossil-based quantitative and qualitative proxies for paleoceanographic conditions. We recommend paleoceanographers to a priori evaluate the (paleo)water depth, oceanographic setting, current strength, and particle aggregation probability for their sedimentary microplankton assemblages.

1. Introduction

Dinoflagellates are a common component of the surface water microplankton community. As part of their complex life cycle, about 20% (Evitt, 1985) of modern dinoflagellate species produce a resting cyst (Zonneveld et al., 2013b). The cyst-producing dinoflagellates lose their mobility at cyst formation, from that time onward they are subject to ocean current transport until they reach the ocean floor. The cyst wall protects the dormant dinoflagellate and is composed of a biopolymer that is relatively resistent to oxic degradation; hatching of the dinoflagelate leaves the dinocyst as a microfossil trace in the sedimentary record if it is preserved.

Dinoflagellate cysts show distinct bioprovincialism in the present-day globally (Zonneveld et al., 2013b), regionally (Matthiessen, 1997; Prebble et al., 2013), and for long-extinct species during time intervals in the geologic past (Bijl et al., 2011, 2013). It was shown that the composition of sedimentary dinoflagellate cyst (dinocyst) species relate to environmental conditions at the surface ocean, which is used to reconstruct past oceanographic conditions. For many cyst species, it is unknown which dinoflagellate produces a specific cyst. As a result, ecologic affinity of a dinocyst species in most cases cannot be derived from its biological producer, the dinoflagellate. Hence, the relationships between the nonmotile cysts and surface conditions are made independent of the taxonomy and biology of the motile dinoflagellates. Both quantitative (de Vernal et al., 1992; Frieling & Sluijs, 2018; Marret et al., 2001) and qualitative (Bijl et al., 2011, 2018;

Crouch et al., 2014; Cramwinckel et al., 2019; Houben et al., 2013; Sluijs et al., 2005, 2006) paleoceanographic reconstructions based on dinocysts exist.

Quantitative reconstructions using transfer functions of modern analogues have been instrumental to reconstruct past ocean conditions (de Vernal et al., 1992; Datema et al., 2017; Matthiessen, 1997). Transfer functions are based on the assumption that a sedimentary microfossil assemblage composition explains part of the variability of environmental conditions. Transfer functions are used to calculate these relationships using a present-day core top data set, which includes surface sediment microfossil data and compares these to the environmental conditions inferred from the directly overlying water. This technique has also enabled to assess paleoceanographic affinities of extinct dinocyst species, by comparing their relative abundance to proxy reconstructions of past sea surface temperature (SST) in the same samples (de Schepper et al., 2011).

However, applications of these quantitative techniques have large uncertainties or scatter in some regions (Prebble et al., 2013) or show unrealistic values in past time intervals, for example, near New Zealand (Marret et al., 2001). This induced large error bars of uncertainty and also reduced confidence in using these techniques to reconstruct past oceanographic conditions. Some challenged the quantitative methods on ecological grounds (Dale et al., 2002) and others on statistical grounds (Telford & Birks, 2009). However, sediment trap measurements indicate that sinking particles could be transported laterally (Chen et al., 2012; Fahl & Nöthing, 2007; Honjo et al., 1982). The lateral particle transport in these sediment trap studies could occur during their trajectory from the surface to the bottom of the ocean. Another view for dinocysts, however, is that they are mainly transported after resuspension, and the cysts in the deep ocean reflect a specific biogeographic zone in shallow coastal waters (where most cysts appear; Dale, 1996). Nevertheless, the lateral transport of the sinking cysts by ocean currents could induce a major uncertainty on their use as a proxy of local environmental conditions.

SST is suggested as the variable that explains most of the dinocyst distributions by multivariate statistics on a global data set of sedimentary distributions (Zonneveld et al., 2013b; which comprises dinocyst assemblage data from 2405 surface sediment sites), and the average surface oceanographic properties of the overlying water. Nevertheless, this relationship shows profound scatter, also for specific dinocyst species. Of course, some dinocyst species will have a more stringent temperature range than other (more generalistic) species. However, the scatter is a commonly seen feature and particularly the broad tailing of species' temperature affinity (toward the cold and/or warm end). Although it could be that dinocysts have relatively broad temperature tolerances, perhaps other factors also play a role in the dinocyst-environmental relationships.

To illustrate the potential of these transportation effects, one can perform a quick calculation. If a sedimentary cyst sunk to 4-km depth, at 11 m/day (which is a typical sinking speed for dinocysts according to Anderson et al., 1985) through the water column with an average horizontal ocean flow speed of ~5 cm/s, it took almost 1 year before the dinocysts reached the ocean floor and could be displaced by up to 1,570 km from its location at the surface. The bias could have major effects on the ability to use sedimentary dinocyst assemblages as proxy for surface ocean conditions. By understanding the surface origin of the cysts in the sediment and quantifying the biases and regional variations of the effects of lateral transport during sinking, improved relations between cyst species occurrence and sea surface conditions can be obtained.

Ocean models have over the recent years become increasingly sophisticated: Ocean general circulation models (OGCMs) resolve eddies (Marzocchi et al., 2015), and coupled biogeochemical models provide more properties of the ocean (Aumont et al., 2015; Yool et al., 2013). Together with Lagrangian particle tracking techniques (van Sebille et al., 2018), the high-resolution ocean models enable quantitative assessment of the biasing effects of lateral transport of sedimentary microfossil assemblages. These developments have now offered the opportunity to assess the bias potential of lateral transport in sedimentary plankton assemblages.

Here, we investigate the potential bias of the relationship between dinocysts (as example of any microplankton fossil group) and surface conditions that can be induced by the lateral cyst transport by ocean currents. We will refer to this bias as the "advection bias" (AB). We will present and discuss the regional difference in the AB. Moreover, we examine the sensitivity of the AB to the sinking velocity assumptions. The local magnitude of the effect of ocean currents on sedimentary cyst distributions will be quantified.

Section 2 describes the data and methods, which are used to model and analyze the transport of the cysts. The first part of section 3 focuses on the global scale. We determine the geographic regions where particle transport is important and perform a sensitivity analysis of these results to the sinking velocity of the cysts.

In the second part of section 3, an analysis of the AB is done for a specific location near Antarctica and a specific species (*S. antarctica*). Finally, section 4 provides a summary and a discussion of the implications of our results for microplankton-based paleoceanography.

2. Data and Methods

2.1. Ocean Flow Field Data

We make use of ocean model simulations to propagate virtual particles. OGCM for the Earth Simulator (OFES; Chi et al., 2018; Masumoto et al., 2004; Masumoto, 2010; Sasaki et al., 2008) provides a three-dimensional flow field for the years 2000–2005 from the edge of the Antarctic continent at 75°S to 75°N with 3-daily output. Since the model has no output north of 75°N, we only show results up to 70°N in this paper. The flow field from OFES is used to calculate the trajectories of sinking particles (similar to van Sebille et al., 2015). Moreover, OFES includes a three-dimensional temperature and salinity field, which are environmental variables that influence the habitat of a dinoflagellate. The model has a 0.1° horizontal resolution with 54 vertical levels and is forced by the National Centers for Environmental Prediction wind and heat/freshwater flux fields.

To study the model dependence of the results, we performed the same analysis with another model: Nucleus for European Modelling of the Ocean (NEMO; Madec, 2016; Storkey et al., 2014; Uotila et al., 2017) for the same years (2000–2005; http://opendap4gws.jasmin.ac.uk/thredds/nemo/root/nemo_catalog.html). The NEMO model has a higher horizontal resolution compared to OFES ((1/12)° horizontally) and 75 vertical layers. The output of this model is 5-daily. Furthermore, it includes the Arctic, as the model uses a tripolar grid, which solves the singularity at the North Pole. However, we only consider results south of 70°N as is done for OFES, to be able to compare the NEMO and OFES simulations. The tripolar grid makes interpolation and calculation of the particle trajectories more difficult, but this is recently made possible (Delandmeter & van Sebille, 2019). The results of the analysis from NEMO can be found in the supporting information.

The spatial resolution of the OFES and NEMO models is high enough to resolve mesoscale eddies. The eddies are important to realistically resolve the dynamics of the ocean currents. For example, the 0.1° is seen as a threshold to realistically simulate the seperation location and other features of the Gulf Stream (Hecht & Smith, 2013). Moreover, eddies are important for the transport of dinocysts, as is the case for the transport of heat (Volkov et al., 2008), salt (McWilliams et al., 2014), and floating particles at the surface (such as microplastics; Fraser et al., 2018). Furthermore, the temporal resolution of the OFES and NEMO model outputs is high enough to calculate the particle trajectories within the flow field. To apply a three-dimensional Lagrangian tracking method, the output of the model results must be of high enough temporal resolution (at least 9-daily for ∼0.1° horizontal resolution Qin et al., 2014).

2.2. Particle Tracking and Analysis

Parcels version 1.0.4 (Lange & Sebille, 2017) is used to release virtual particles at the bottom of the OGCM and calculate their trajectories back in time (https://zenodo.org/record/1402023). Parcels computes the trajectories by

$$\vec{x}(t+\Delta t) = \vec{x}(t) + \int_t^{t+\Delta t} \vec{v}(\vec{x},\tau)\mathrm{d}\tau + \vec{C}\,(z)\,\Delta t, \tag{1}$$

where $\vec{x}(t)$ the three-dimensional position of a particle at time t, $\vec{v}(\vec{x},t)$ the flow velocity at location $\vec{x}$ and time t, $\vec{C}\,(z)$ is the sinking velocity, and z the vertical coordinate. We add the sinking velocity to the vertical velocity field (obtained from the ocean model) to make sure that the particles sink to the bottom while passively advected. Coriolis and inertial effects on the particles are small and neglected (Monroy et al., 2017). Moreover, it is essential that the flow field is three-dimensional (i.e., also includes the vertical velocity), because the sinking speed of particles can be of comparable magnitude to the vertical velocity. We release the particles at the bottom of the ocean. This allows us to compare these particles directly to surface sediment sample data. Therefore, we use $\Delta t < 0$, such that the particles are tracked back in time.

To analyze the trajectories of the sinking particles in physical space and the probability that particles move from some location at the surface to some other location at the bottom of the ocean, we use a surface-bottom 'transportation' matrix (T). The bottom of the ocean Y is divided into the boxes $\{B_i\}_{i=1}^{N}$ and the surface of the ocean (or any other horizontal layer within the ocean) Z is divided into the boxes $\{U_j\}_{j=1}^{N}$ (see Figure 1).

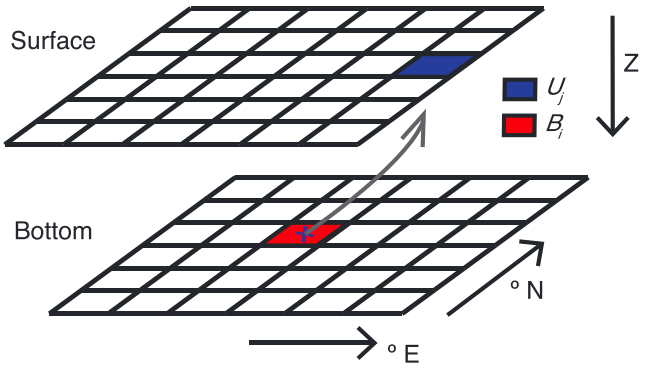

Figure 1. Illustration of the surface-bottom transportation matrix. The transportation matrix contains the probabilities that a particle that is found in bottom box B_i came from box U_j at the surface, for all (i, j).

Particles are released at the bottom of the ocean at uniformly distributed locations and every 5 days. The probability that a particle, which is initialized at the bottom in any box B_i, reaches the surface in box U_j within the total time period considered is calculated according to

$$P_{ij} = \frac{\#\{y : y \in B_i \text{ and } T(y) \in U_j\}}{\#\{y : y \in B_i\}}. \quad (2)$$

Here $T(y) : Y \rightarrow Z$ maps a particle y, which is released at the bottom to the surface box where the cyst once formed at the surface. Hence, P_{ij} estimates the probability that a particle that is measured in box B_i at the bottom comes from box U_j at the surface where it once formed. This matrix allows us to investigate the validity of the assumption that particles sink vertically to the bottom up to a degree of uncertainty, which is determined by the size of the boxes. Moreover, we can quantify the ocean surface area that is spanned by a sediment sample site in any bottom box by summing over the surface area of the connected surface boxes, which also depends on the choice of the box size. Here, we release particles at a $1° \times 1°$ grid at the ocean floor every 5 days for 6 years ($\sim 10^7$ particles in total) and use $2° \times 2°$ boxes for the bottom and surface boxes of the transportation matrix.

Although this particle tracking method could be applied to any sinking particle, to set an example, we specifically track sinking dinocysts in this paper. This requires the incorporation of some dinocyst-specific assumptions and boundary conditions. Before dinoflagellates form their cyst, they are active swimmers with velocities compared to the speed of the currents (Smayda, 2002). This means that dinoflagellates can maintain their position in surface waters with, for them, favorable conditions. However, if the dinoflagellates form their cyst at the "encystment location," they lose their mobility and start sinking. For this reason, we track the particles back in time until they reach their encystment location. As an encystment location we generally choose the location where the particles first reach a depth of 10 m in the back trajectory calculation. Although not much is known about the exact encystment depths of the species, it is often assumed to be at the surface. In order to investigate the dependence of the model results to our choice of encystment depth, we perform a simulation with an encystment depth down to 100 m (see the Figures S7 and S8 of the supporting information), but the sensitivity of the results to encystment depths was found to be much smaller than the sensitivity to sinking speeds.

Choosing a realistic sinking speed is not straightforward. Once formed, dinocysts tend to behave like fine silt particles (Dale, 1976) and sink with a velocity in the order of 6–11 m/day based on the specific density, shape, and buoyancy measurements of several cyst species with fresh cell contents (Anderson et al., 1985; without fresh cell contents, the cysts could be lighter and sink slower). The formation of aggregates can significantly enhance sinking speeds of particles, which reduces the AB. Aggregates can form either by binding of particles, often with help of sticky substances such as transparent exopolymer particles (Azetsu-Scott & Passow, 2004; Bach et al., 2016), or via fecal pelletting. Moreover, aggregate sizes could change within the water column while sinking (Jokulsdottir & Archer, 2016). Particulate organic carbon export flux and flux efficiency (flux relative to surface water primary production) is varying spatially (Tang et al., 2019) due to varying ballasting effect of lithogenic particles (Rixen et al., 2019), or variations in particle composition (Schmidt et al., 2014). Although there is a strong bias of larger, fast-sinking particles contributing to the particulate organic carbon that reaches the seafloor (Riley et al., 2012), because the sinking speed and particle size reduce the biomineralization process along the sinking trajectory, it was shown that at several locations, both marine snow (Alldredge et al., 1998) and aggregates (Mudie, 1996) are devoid of dinocysts. This may be because of two reasons. First, it was suggested that zooplankton select against dinocysts for their lack of nutritional value (Montresor et al., 2003). Second, formation of large particles is the consequence of surface water primary production peaks (Schmidt et al., 2014). It is unlikely that these dinoflaggelates encyst during these primary production peaks, since they reproduce asexually when plenty of nutrients are available and return to dormancy when conditions worsen. As a result, encystment will occur at times when surface water primary production is low, and particles avoid the fast-track to the sea bottom in large particles. This was clearly demonstrated for sediment trap studies in the Arabian Sea, where dinocyst flux was highest in low primary production seasons (Pospelova et al., 2018). However, whether dinocysts sink as being part of

marine snow could be species specific, as was shown in areas with exceptionally high cyst fluxes (~50,000 cysts per square meter per day; Bringué et al., 2018, 2019).

All in all, we conclude that it is unlikely that dinocyst sink via large aggregates, but it remains challenging to realistically and adequately incorporate the observations on sinking speeds into our simulations. In order to evaluate the effect of sinking speed assumptions on the AB, we perform a sensitivity test by which we simulate particle transport under a suite of realistic constant sinking speeds of both individually sinking dinocysts (Anderson et al., 1985) and aggregates (Berelson, 2002). Moreover, aggregates seem to increase sinking speed with water depth (Berelson, 2002), probably due to increasing size and mass of the aggregates, and decrease of buoyancy. In order to investigate this scenario, we also perform two simulations (SC1 and SC2) where we make the sinking speed $\vec{C}(z)$ of a particle dependent on the depth of the particle (z), as follows: In SC1, the sinking speed is 6 m/day between 10- and 100-m depths and increases linearly between 100 and 2,000 m up to 45 m/day. SC2 is similar to SC1, but the sinking speed increases further between 2,000- and 3,500-m depths up to 65 m/day. So the sinking speed in SC1 and SC2 are respectively defined as

$$\vec{C}_1(z) = \begin{cases} 6 & 10\,\mathrm{m} < z \le 100\,\mathrm{m} \\ 6 + \frac{(45-6)(z-100)}{2000-100} & 100\,\mathrm{m} < z \le 2,000\,\mathrm{m} \\ 45 & z > 2,000\,\mathrm{m} \end{cases},$$

$$\vec{C}_2(z) = \begin{cases} 6 & 10\,\mathrm{m} < z \le 100\,\mathrm{m} \\ 6 + \frac{(45-6)(z-100)}{2,000-100} & 100\,\mathrm{m} < z \le 2,000\,\mathrm{m} \\ 45 + \frac{(65-45)(z-2,000)}{35,00-2,000} & 2,000\,\mathrm{m} < z \le 3,500\,\mathrm{m} \\ 65 & z > 3,500\,\mathrm{m} \end{cases}.$$

The sensitivity study provides ways to portray the bias effect for various sinking speeds, making our simulations applicable to any particle. We apply SC2 as the most plausible sinking speed scenario for dinocysts. A constant sinking velocity of 6 m/day (see Figures S1, S3, and S5–S9 of the supporting information) is considered as an upper bound of the magnitude of the lateral particle transport, because the lateral particle transport is expected to decrease if the sinking speed increases and 6 m/day is the lower bound of individually sinking cysts (Anderson et al., 1985). The sinking scenarios ignore any seasonal dependence of the sinking speed and the dinocyst productivity.

Once the virtual dinocysts are tracked with a certain sinking scenario and encystment depth, the AB has to be determined. The ocean surface water conditions where the cysts come from (i.e., where the model simulates the encystment location) are compared to the environment in the surface waters above the release location at the bottom (where cysts are found in a sediment sample). We express environmental conditions at the surface as probability density functions (PDFs). The first PDF is inferred from the values of the environmental variable at the surface where the virtual particles first reach the encystment location (10-m water depth) in the model. This type of PDF is referred to as the "advection PDF" (APDF). The second PDF can be determined from the environmental variable that evolves in time at the fixed surface location overlying a sample site. This PDF is referred to as the "local PDF at a fixed location" (LPDF; blue in the figures throughout the paper); see, for example, Figure 2.

In this paper, we use two measures for the AB (AB1 and AB2) between the APDF and the LPDF. AB1 and AB2 are defined as the difference between tail of the APDF with respectively the LPDF's mean (often used in quantitative and qualitative methods) or the LPDF's tail (part of the difference between APDF tail to LPDF mean which is caused by lateral particle transport). We define the tail by the 5th or 95th percentile. Hence, we use the following measures for temperature AB:

$$\begin{aligned} \mathrm{AB1}^{\mathrm{warm}} &= \mathrm{percentile}(\mathrm{APDF}, 95) - \mu_{\mathrm{LPDF}}, \\ \mathrm{AB1}^{\mathrm{cold}} &= \mathrm{percentile}(\mathrm{APDF}, 5) - \mu_{\mathrm{LPDF}}, \\ \mathrm{AB2}^{\mathrm{warm}} &= \mathrm{percentile}(\mathrm{APDF}, 95) - \mathrm{percentile}(\mathrm{LPDF}, 95), \\ \mathrm{AB2}^{\mathrm{cold}} &= \mathrm{percentile}(\mathrm{APDF}, 5) - \mathrm{percentile}(\mathrm{LPDF}, 5), \end{aligned}$$

where μ_{PDF} is the mean and $\mathrm{percentile}(\mathrm{PDF}, k)$ is the kth percentile of the PDF. The tail of the APDF informs about the environmental conditions of far-traveled particles. The tails of the APDF are used here as a

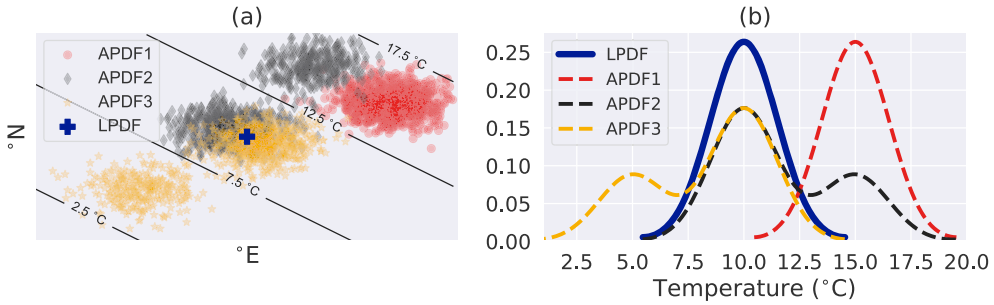

Figure 2. Schematic of the LPDF and APDF for three different oceanographic settings resulting in a different temperature APDF. (a) Map view. The blue plus represents the location of the sediment sample site. Red, black, and yellow are the backtracked locations in respectively the first, second, and third oceanographic setting. The contours show the annual average sea surface temperature. (b) The LPDF and the APDFs of sea surface temperature for the three backtracking scenarios. In the first oceanographic setting (red, APDF1), all backtracked particles come from a warmer region, leading to a warm shift of the APDF with respect to the LPDF. The second (black, APDF2) and the third (yellow, APDF3) oceanographic setting result in, respectively, warm and cold tail with respect to the LPDF. APDF = advection probability density function; LPDF = local probability density function.

measure of the AB for two reasons. First, because we only model the area where the cysts in a sediment core could have come from as a result of the transport by ocean flow. In reality, the productivity of dinocysts at the surface is not uniform in space and time, and the dinocysts do not necessarily originate from the model predicted locus (e.g., because the ecological preference of the dinocyst does not agree with the model predicted locus). Therefore, we use the tail to obtain a confidence interval with a lower and an upper bound of species properties in a sediment sample. Second, transfer functions of modern analogues, which quantitatively relate sedimentary dinocyst assemblage data to environmental conditions, are very sensitive to extreme occurrences (i.e., occurrences of species outside of their typical habitat with low abundance) and therefore greatly affect the reliability of the proxy (Ohlwein & Wahl, 2012).

3. Results

We first distinguish regions where lateral particle transport is important from those where it is not. Furthermore, we perform a sensitivity analysis on sinking speed to account for uncertainties in our assumptions on sinking behaviours of dinocysts. Then we show one case study of a specific sediment sample site with a relatively large AB. Finally, we indicate what kind of implications the particle transport could have for the interpretation of dinocyst species and their ecological affinities.

3.1. Global Analysis

We first investigate the lateral transport of the particles using the transportation matrix, without considering the AB of environmental variables. In general, we find a relatively small effect of the particle transport by currents at shallow water depths (Figure 3). At those areas, most released particles come from the overlying surface grid box (Figure 3a), a sediment sample relates to a relatively smaller surface area (Figure 3b) and the average traveled horizontal distance of particles released in the bottom boxes is lower (Figure 3c). Hence, the assumption that particles sink vertically to the bottom is more plausible in shallow, continental shelf areas.

The lateral particle transport is relatively large in deep ocean basins and further enhanced near strong currents, such as the western boundary currents and near the Antarctic Circumpolar Current (ACC). The large surface area (Figure 3b) is horizontally distant from the release location at the bottom at the ACC, because the ACC strongly transports the particles eastward and the travel distance is large (Figure 3c). On the other hand, near western boundary currents, the surface area is closer to the release location, because the vertically integrated currents are weaker compared to the ACC. Locations with relatively large lateral (latitudinal) travel distances that are mapped to a small surface area are rare, because the large travel distances require strong currents, and strong currents are often accompanied by eddies. These eddies increase the variability of the direction and strength of transport pathways and therewith the surface area which is mapped to a bottom box.

Changing the sinking speed assumption for the particles does not affect the geographical structure of where the lateral transport is important. However, the sinking speed assumption does influence the magnitude of

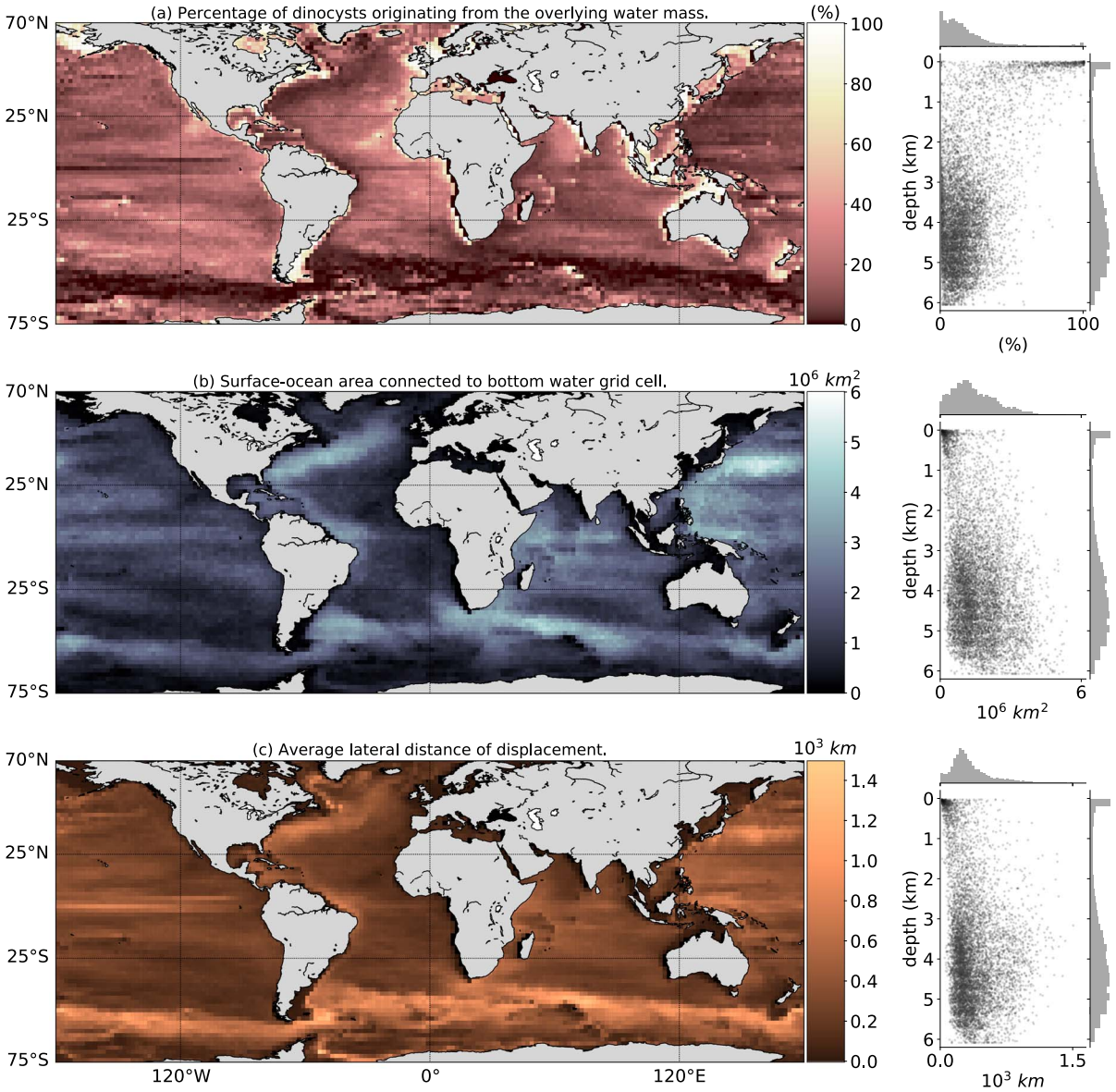

Figure 3. Transportation matrix results with 2° × 2° surface and bottom boxes with sinking scenario SC2: Geographic plot (left) and scatterplot against depth of the bottom boxes (right). (a) The probability that a particle ends up in the same box at the surface as it is released at the bottom (the diagonal of the transportation matrix). (b) The surface area of all grid boxes at the ocean surface that a bottom box is connected to. (c) The average horizontal distance between the release location and the backtracked encystment location (averaged for a bottom box). See Figures S5 and S6 of the supporting information for the same figure with 6 m/day sinking velocity instead of SC2.

the lateral particle transport distance and therefore the magnitude of the potential bias. The lateral particle transport distance reduces if the sinking speed increases (Figure 4). However, locally the particle transport distance can still be substantial at higher sinking speeds. The lateral particle transport distance becomes 0 if the sinking speed approaches infinity. Most sites in the core top data set (Zonneveld et al., 2013a) are relatively close to the coast and therefore in relatively shallow regions. Hence, the particle transport is on average lower at the sample site locations compared to the global average ocean. The results for the linearly increasing sinking scenarios (SC1 and SC2) yield similar results, so the increase in sinking speed of SC2 below 3,500-m depth compared to SC1 does not influence the particle transport on average. More importantly, the horizontal particle transports for SC1 and SC2 are not clearly higher compared to the constant 11-m/day simulation, which indicates that a large part of the transport takes place in deeper than ~344 m in the 11-m/day simulation (in SC1 and SC2 the sinking speed exceeds 11 m/day at depths $z \gtrsim 344$ m). It

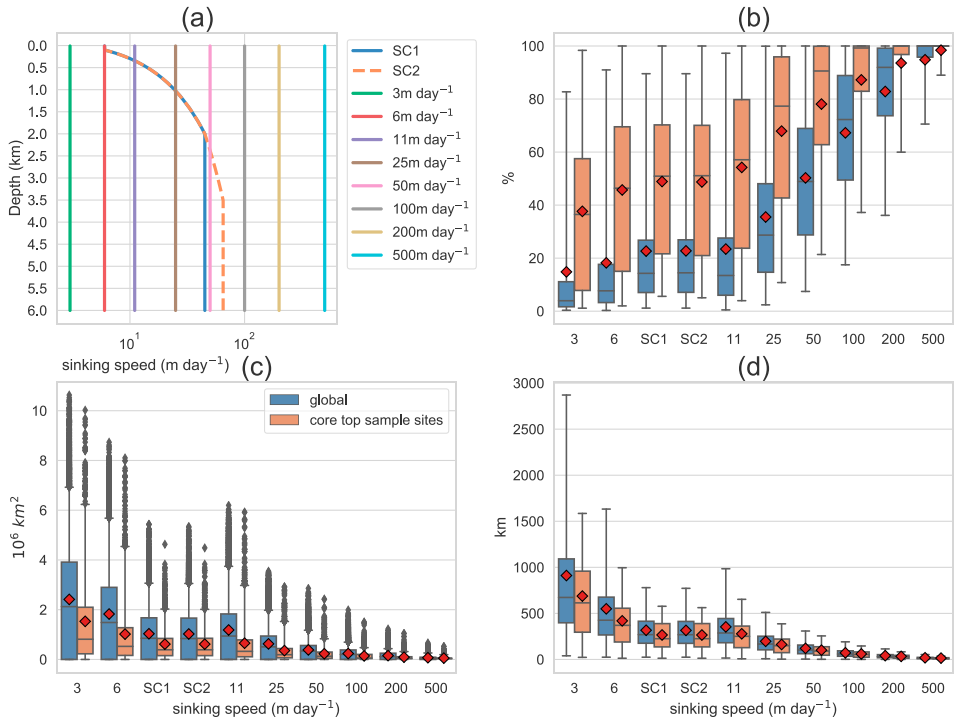

Figure 4. Sensitivity analysis of the results in Figure 3 versus sinking speed. (a) Illustration of the sinking speed scenario's (with constant sinking speeds and SC1, SC2 with sinking speed dependent on depth), which are used in the sensitivity analysis on sinking speed (note that the horizontal axis is logarithmic). Boxplots show the 5th, 25th, 75th, and 95th percentiles around the median of (b) the probability that a particle ends up in the same box at the surface as it is released at the bottom (diagonal of the transportation matrix), (c) the surface area of all grid boxes at the ocean surface a bottom box is connected to (including outliers), (d) the average travel distance from a bottom box. For all defined bottom grid boxes as in Figure 3 in the ocean (blue) and for the locations of present-day surface sediment samples (orange). The red diamonds are the mean of the distribution.

also means that even under the aggregate sinking speed velocities available from the literature, transport of dinocysts still plays an important role.

3.2. Temperature and Salinity AB

While the amount of lateral transport of sinking particles can be relevant for a substantial part of the ocean, the environment is not necessarily different at the location where the cysts are transported from, compared to the local surface conditions. That is why we will now compare the tails of the temperature/salinity APDFs with the mean of the temperature/salinity LPDFs: the advection bias (AB1).

The temperature AB1 is relatively large (up to ±16 °C) in specific regions, such as the western boundary currents and north of the Southern Ocean (Figure 5), it is smaller (than ±2 °C) in other regions, such as near the equator. For salinity, the AB1 is large (up to ±4 PSU; Practical Salinity Unit) in regions with ice melt and near river outflow regions such as near India and the Amazon, while the AB1 is low (smaller than 0.5 PSU) in the open ocean and away from the strong western boundary currents. Interestingly, not all regions with large transport effects have a large temperature AB: A strong current does not always lead to a large AB, such as in parts of the ACC. The relatively low AB is induced in these regions by a lower temperature or salinity gradient along the transport pathways of the particles, for example, the transport in parts of the ACC is zonal and the zonal temperature gradient is low.

The southeast of Brazil (at the Uruguayan margin) is an example with large temperature and salinity AB. In this dynamic region, the northward branch of the ACC (the Malvinas current) and the southward flowing Brazil Current meet, and locally, large temperature and salinity gradients exist (Matano et al., 2010). The APDF and also the LPDF therefore have a non-Gaussian shape in this area. As a result, our model simulations predict that a surface sediment sample in this area could contain species which represent SSTs of either 16 °C colder (Figure 5a) or warmer (Figure 5b) compared to the local average (mean of LPDF). Although cyst

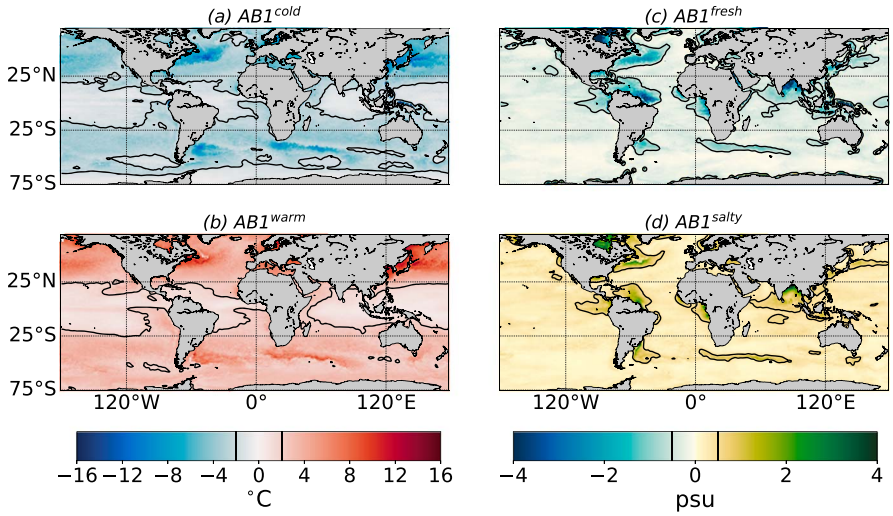

Figure 5. The tails of the advection probability density functions with SC2, compared to the local average (mean local probability density function). The local average is subtracted from the (a) 5th and (b) 95th percentiles for sea surface temperature of the advection probability density function. (c, d) The same as (a) and (b) but for salinity. The black contours are the ±2 °C or ±0.5-PSU levels.

assemblages in higher latitudes naturally include warmer species that exist in summer together with colder ones from winter, the example, indicates that cyst transport could induce a strong AB here. Another interesting example where the LPDF of temperature has a non-Gaussian shape is the Kuroshio current, because the path of the current is bimodal (Schmeits & Dijkstra, 2001).

The AB in terms of the difference between the APDF and LPDF tails (AB2) also shows considerable dependence on sinking speed assumptions (Figure 6), for example, comparing the boxplot with sinking speed 6 m/day with SC2 (Figure 6a): It is at 6 m/day very unlikely (below 1% probability) that the sedimentary dinocysts that are found at an arbitrary location are related to a habitat at the surface 6 °C colder than the cold tail of the local temperature (LPDF) due to the particle transport, while for SC2 this is 2.5 °C. Hence, the AB2 reduces quickly if the sinking speed is larger.

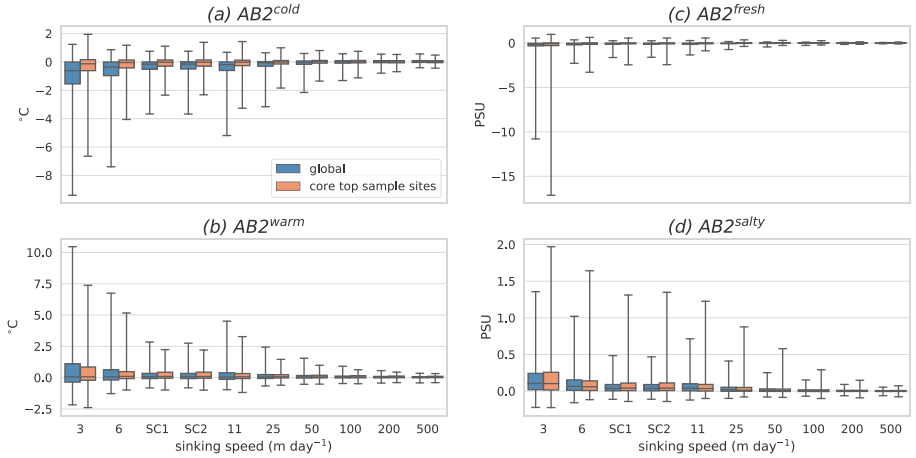

Figure 6. The sensitivity of the displacement of the probability density functions tail due to particle transport on sinking speed (SC1 and SC2 are the two sinking scenarios with increasing sinking speed with depth). Difference of the (a) 5th and (b) 95th percentiles of the temperature advection probability density function from the same percentile of the local probability density function. (c, d) The same as (a) and (b) but for salinity. The boxplots show the 1st, 25th, 50th, 75th, and 99th percentiles around the median for all locations (blue) and the dinocyst sample locations in Zonneveld et al. (2013a; orange).

The tails of APDFs and LPDFs differ little at about 50% of the locations (up to ±0.5 °C or ±0.1 PSU for SC2). At some locations, however, the tails of the APDF could become ~3 °C warmer or colder and ~2.5 PSU fresher or ~0.5 PSU saltier at SC2. The AB2 for salinity is asymmetric here, because of the backtracking of particles near outflow regions of rivers: A particle that is released in the ocean could end up in a fresh river outflow region after backtracking, leading to a strong fresh AB2. On the other hand, a particle that is released in the river outflow region will likely end up in the same region due to the direction of the current, which leads to a small AB2. The change in the tails decreases quickly for higher sinking speed at the locations where the particle transport matters most. Eventually, this change converges toward 0 for all variables and all locations if the sinking speed increases up to 500 m/day. It is interesting to note that the transport of currents does not always cause the tail of the PDF to be fatter and can also decrease the tail and result in a more confined PDF (with a lower kurtosis). In these cases, the spread of an LPDF is large due to a passing front (such as the Kuroshio current), while the backtracked particles come from a surface location with more constant properties. Most interestingly, however, the lateral particle transport is not important in regions where many large aggregates form, although it can be relevant under realistic aggregate sinking scenarios SC1 and SC2. Hence, it is crucial to get a better understanding for mechanisms and factors that control the sinking velocity of particles.

To summarize these global results, the importance of the particle transport at a certain location on the sea floor depends on five factors. First, the water depth at the sample site and second the strength of the current, which both control the distance that cysts travel before they reach the bottom of the ocean. Third, it is the horizontal spread of directions a cyst could travel within the flow field, which determines the surface area at the ocean surface, which is measured at a sample site. Fourth, it is the gradient of the environmental variable of interest (such as temperature and salinity) along the trajectories that cysts can travel within the flow field. Fifth, it is the aggregation probability of the microplankton, which influences the sinking speed. We determined in which regions these factors create the largest AB and the sensitivity of the AB to the sinking velocity of the cysts. We further conclude that all these factors are important to take into account when looking at sedimentary microplankton data, also in sediment cores that aim to reconstruct past oceanograpgic changes. To investigate whether these factors are of importance in the past record, one could apply the backtracking method to an ocean model, which simulates the past ocean circulation.

In order to test for model dependency of our global results, we also performed the same simulations with the NEMO model (see Figure S1 through S4 of the supporting information). The model dependency test shows geographic differences between the simulations, because the exact pathways of ocean currents are model dependent. These geographical differences induce larger particle transport and larger AB in the NEMO simulation compared to OFES for the sediment sample site locations. However, the global average of the particle transport by ocean currents is similar (according to the sensitivity study on sinking speed Figure S2). Moreover, the general conclusions regarding the global transport of sinking cysts and the AB are similar.

3.3. Case Study in the Southern Ocean

From the global simulations we were able to identify regions where the particle transport is important in terms of the relation of sedimentary cysts with environmental variables at the surface of the ocean. One of the regions with important particle transport is the Southern Ocean, because a large part of the Southern Ocean has a strong AB due to the combination of strong currents and strong latitudinal SST gradients. We will study how the particle transport can be important for the interpretation of a particular sample site as well as the global ecological affinity of two specific species: *Selenopemphix antarctica* and *Spiniferitus delicatus*.

3.3.1. A Subtropical Southern Ocean Surface Sediment Site

Station 3627 (Zonneveld et al., 2013a; Figure 7) is an example of a Southern Ocean sediment sample site at almost 5-km water depth. The temperature LPDF at this location, which is computed from the evolution of SST at the sediment sample location over the six simulated model years, has a unimodal shape. The (blue) LPDF shows that the SST is 9 ± 1.5 °C (the 90% confidence interval around the average, which gives a range of species properties that could be measured in the sediment sample). Hence, if one assumes that the cysts sunk vertically to the ocean floor, the sediment sample relates well to the average of the LPDF. Furthermore, station 3627 is located close to the subtropical front (Orsi et al., 1995) and remote from sea ice and icebergs (Tournadre et al., 2012).

Moreover, the sediment sample of station 3672 contains a diverse dinocyst assemblage (Figure 7d). Some of these species are typically abundant in temperate regions similar to the local conditions (but are sometimes

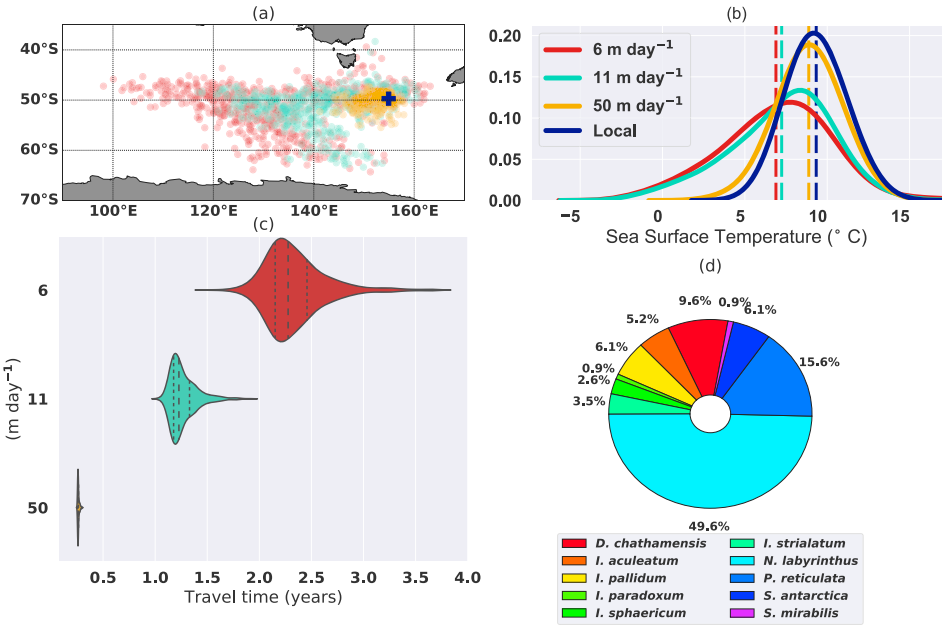

Figure 7. Example of the particle backtracking for station 3627 (154.91°E and 49.71°S) at approximately 4,730-m depth. The particles are released at the ocean bottom and tracked back in time with a sinking speed of 6 m/day (red), 11 m/day (green), and 50 m/day (yellow; ~600 particles for each sinking speed scenario). (a) The release location at the blue cross and in red/green/yellow the locations where the particles reach the encystment location of 10 m. (b) The probability density functions, which are infered from the evolving temperature at the sea surface location at the station (during the 6 years of the simulation; local probability density function in blue) and for the sea surface temperatures when a particle reaches the encystment location after backtracking in the simulation (advection probability density functions in red/green/yellow). The vertical dashed lines are the probability density function means. (c) Distribution of the time that particles took to sink (the vertical dashed lines show the median and quartiles). (d) The relative abundances (%) of species found in the surface sediment at station 3627.

also found in warmer areas), for example, *Dalella chathamensis, Impagidinium aculeatum, Impagidinium paradoxum*, and *Spiniferitis mirabilis* (Zonneveld et al., 2013b). On the other hand, *Nemaosphaeropsis labyrinthus* and *Pyxidinopsis reticulata* are particularly abundant at ocean frontal system localities, and particularly the subtropical front. *Impagidinium pallidum* occurs in high abundance in polar regions, although low abundances in other regions have also been reported (Zonneveld et al., 2013a). Finally, *S. antarctica* is only very high in abundance closer to Antarctica south of the polar front and within the sea ice zone (Prebble et al., 2013; Zonneveld et al., 2013a), has been reported in high abundance in Holocene polynya-derived drift sediments (Hartman et al., 2018) and is used as proxy for sea ice conditions for the geologic past (Bijl et al., 2018; Houben et al., 2013). However, *S. antarctica* also occurs in the sediment sample of station 3627 with 6.1%.

From the local conditions of station 3672, *S. antarctica* and *I. pallidum* are not expected in the sediment samples. However, surface Ekman transport induces northward surface currents, being part of the meridional overturning circulation (Marshall & Radko, 2003), which could transport particles northward, from across the ACC. Hence, cold species could be transported from the far south to the site, while warmer species did not travel far, because of limited southward water transport in the region. When looking at our particle back trajectory calculations, we note under assumptions of sinking speed that a fraction of the particles come from colder waters close to Antarctica. The cold tail of the APDF represents this additional input of colder water species to the site. The 90% confidence interval around the median of the APDF is 1–12 °C (if the sinking speed is 6 m/day).

These simulations also allow for investigation of the travel time of the particles. The travel time of particles ending up at station 3672 exceeds 1 year for all particles in the 6- and 11-m/day simulations. Furthermore, the spread of the travel time between the particles increases if the sinking speed decreases. The spread of the travel time is induced by the varying vertical velocities of the flow field. This means that seasonal variations

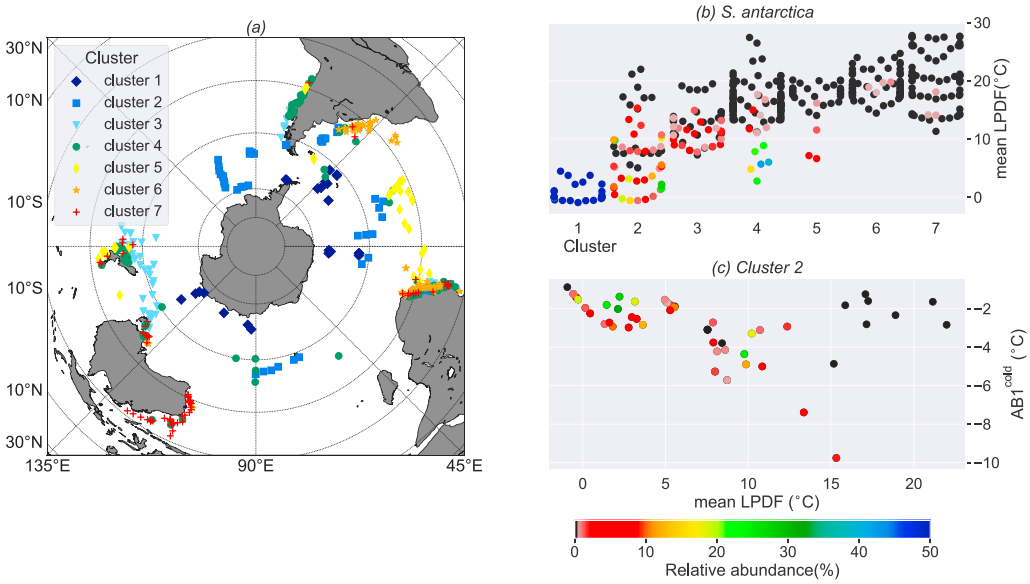

Figure 8. *Selenopemphix antarctica* compared to clusters with similar dinocyst assemblages. The clusters are derived with the *k*-means algorithm as in Prebble et al. (2013), for the surface sediment samples south of 12°S. (a) Map of the sediment sample sites and their cluster. (b) Swarm plot of the local temperatures (mean local probability density function) of the surface sediment samples in specific clusters. (c) The local average temperature versus the cold AB1 (with SC2) for the sediment samples of cluster 2. The color is the relative abundance of *S. antarctica* in the surface sediment samples in (b) and (c) (black if the relative abundance is 0).

are averaged out in dinocyst assemblages at this location, on top of the typical mixing of accumulation from multiple years within the surface sediment sample itself.

3.3.2. Ecological Affinities of Specific Species

The skewness of the APDF in the surface sediment sample of station 3672 is not unique. A mismatch between dinocyst core top sediment samples and overlying sediment traps is also measured in some other areas of the Southern Ocean, indicating that lateral transport affects the sediment samples (Harland & Pudsey, 1999). The question is whether all samples with cold-water affiliated species have a cold tail in the APDF (which indicates that these species could have been transported to the sites) or whether these species actually occur in relatively warm regions with lower abundances. Therefore, we cluster the sediment samples in the Southern Ocean based on their species constituents and investigate the tailing of the samples' APDFs in these clusters (Figure 8). We compare the tailing of the APDFs in these clusters to the sea-ice-affiliated *S. antarctica*.

We choose to focus on *S. antarctica* here, because its occurrence in low to moderate abundance north of the polar front and around New Zealand (Crouch et al., 2010; Prebble et al., 2013) led to questioning of the validity of *S. antarctica* as proxy for polar conditions. It was further reported in higher abundance in Pleistocene glacial deposits offshore New Zealand, which caused quantitative reconstructions using dinocyst-based modern analogue technique to suggest much colder glacial SSTs for that region than anticipated by SST reconstructions with foraminifera (Marret et al., 2001). Thus far, these authors have considered *S. antarctica* to be part of the in situ, pelagic sedimentary component and have interpreted it to be originating from the overlying water mass. However, it could be that *S. antarctica* was actually transported to the site via ocean currents, from the polar front area.

Prebble et al. (2013) statistically clustered Southern Hemisphere dinocyst assemblages from the surface sediment sample data set into seven clusters. *S. antarctica* is found in multiple clusters of similar dinocyst assemblages. *S. antarctica* dominates cluster 1, which only contains samples in cold areas close to Antarctica. As expected, the AB is lower in cluster 1 compared to other clusters, because the ACC isolates these sample sites, which prevents southward transport of subtropical species. More interesting are the clusters which do contain *S. antarctica* and also consist of sample sites in relatively warm areas (e.g., cluster 2 and cluster 4). First of all, we note that in clusters 3–5, the stations with *S. antarctica* come from the stations with relatively cold LPDF (Figure 8b). If the occurrence of *S. antarctica* in these sample sites is caused by

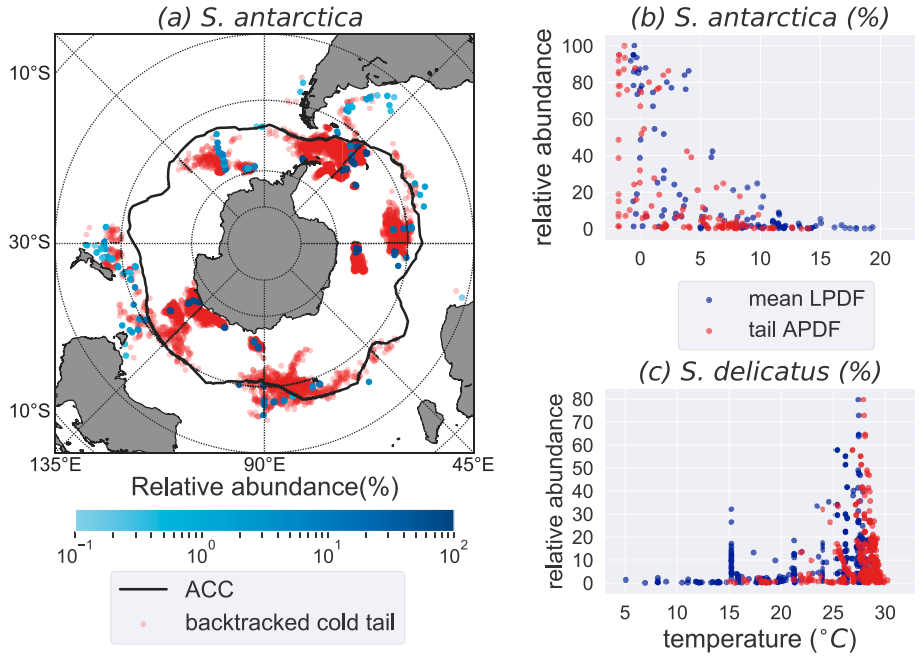

Figure 9. Biasing effects of ocean currents on dinocyst distributions (with SC2). (a) In blue the sediment sample sites where *Selenopemphix antarctica* is found, where the color represents the relative abundance (*n*) of *S. antarctica* in the sediment sample. In red a selection of the locations where the virtual particles reached the surface after backtracking from the sediment sample sites. We have only plotted the surface ocean locations where the temperature was lower than the *n*th percentile of the temperature APDF (see Figure 7) associated with the sediment sample site where the particle was released. Hence the higher *n* at a site, the larger the part of the cold tail of the APDF is considered. The ACC location (black line) is determined by the latitude with strongest average flow at every longitude. (b) In blue the mean of the temperature LPDF of a site against the relative abundance of *S. antarctica* at the site. In red the (1/2)*n*th percentile of the temperature APDF of a site against the relative abundance (*n*) of the site. (c) Same as (b) but for *S. delicatus* and the (100−1/2*n*)th percentile in order to represent the warm tail of the probability density function. ACC = Antarctic Circumpolar Current; APDF = advection probability density function; LPDF = local probability density function.

transport, one expects a relationship between the local temperature and the cold tail of the APDF. This implies that any site with a relatively high local temperature has either an APDF with a relatively large cold tail (colder AB1) or a lower relative abundance (or absence) *S. antarctica*. This is the case in cluster 2 (Figure 8c). To conclude, we see that in most regions a sediment sample site contains relatively more *S. antarctica* if (a) the local average temperature is low and/or (b) the cold AB1 is large.

These observations support the idea that one could misinterpret the ecological affinity of species with relating sedimentary cyst assemblages to the directly overlying water. We will further substantiate the quantitative effects of this for *S. antarctica*. We apply the backtracking method at all sites where *S. antarctica* is found and only consider the backtracked locations, which belong to the coldest *n*th percentile associated with the site (here *n* is the relative abundance of *S. antarctica* in the sample; Figure 9a). Under the assumption that the relative abundance scales with the amount of cold backtracked particles, we deduce that the surface locations where *S. antarctica* comes from are almost exclusively constrained within or south of the ACC. It is therefore plausible that *S. antarctica* at temperate to subtropical sites actually originated from colder regions and was transported to the sediment sample location. To further illustrate the consequences of this interpretation, we adjust the SST of each of these sample sites from the mean of the LPDF to the temperature according to their APDF's cold tail (the 1/2*n*th percentile of the backtracked temperatures). This approach increases the adjustment of the LPDF according to the amount of cold tailing in the APDF and the relative abundance of *S. antarctica n*: The larger the cold tail in the APDF and the lower *n*, the more the temperature of that sample location is adjusted. In this approach, we can constrain the temperature range of *S. antarctica* occurrence to 0–13 °C instead of the original 0–20 °C (Figure 9b); dominant occurrences (>20%) even only occur at SSTs between 0 and 5 °C.

Similarly, we show that the warm species *S. delicatus* (which is also shown to have affinity with high nutrient levels Dale et al., 2002) could be a warmer species than previously thought. From the means of the LPDFs (blue points in Figure 9c) it seems that *S. delicatus* has some local preference at around 16 °C (Zonneveld et al., 2013b) and does also occur in low abundances at sites with a much colder temperature in the overlying waters. Particularly interesting in this case is the suite of samples with overlying waters around 15 °C, and relative abundances of *S. delicatus* ranging between 0% and 37%. However, we observe in the same figure that all sites where *S. delicatus* is found are related to a temperature APDF, which contains a tail toward warm regions. Following this logic, and by applying the same approach as for *S. antarctica* but then for the warm tails, the temperature affinity range of this dinocyst can be constrained to 17–30 °C instead of 4–30 °C (Figure 9c), with a strong affiliation of high (>30%) abundance of *S. delicatus* to SSTs above 24 °C. Particularly, the cluster of sample sites with high abundance of *S. delicatus* at 15 °C has apparently a strong warm tail: The temperature of all these sample sites was adjusted to above 24 °C. To conclude, both the APDF tailing of *S. antarctica* and *S.delicatus* serve as examples of how the particle tracking method can be used to suggest ecological affinities of microplankton species taking particle lateral transport into account. More investigations of specific species of dinocysts and their ecologic affinity can be made available upon request. For other microplankton groups, slight adjustments of the underlying assumptions need to be made in order to make this fully applicable.

4. Summary and Discussion

We have investigated how lateral dinocyst transport by ocean currents influence sedimentary signals preserved in microfossil assemblages used to reconstruct past climate. Virtual particles are released at the bottom of the ocean in an OGCM. The particles were tracked back in time, to compute where and at what kind of surface environment they potentially came from for certain sinking scenarios.

First, we identified locations where the particle transport is low (e.g., shallow and equatorial regions) and regions with relatively large particle transport (e.g., western boundary currents and ACC). However, even if we found that the transport of particles is large in space, the environment is not necessarily different from the local surface environment. The temperature AB is typically large in the proximity of ocean fronts (e.g., subtropical front and Labrador current), as well as regions where currents flow meridionally (Gulf Stream). A sensitivity analysis on the sinking velocity showed that the transport of particles reduces if the sinking speed increases as expected. In regions with a high degree of aggregate formation, lateral cyst transport will be limited. However, even under linearly increasing sinking speed assumptions based on sediment trap measurements, transport has a profound influence on the sedimentary dinocyst assemblage composition.

Next we identified a specific station in a region where the particle transport is important. Particles were transported from a colder area to the station. The example of dinocyst species *S. antarctica* at this station showed that a sediment sample is not always related to the average environment of the surface above it. Moreover, the extremes of the environment after the backtracking of particles can be important. In the case of *S. antarctica* this was the cold extreme of the PDF, which includes the advection of the cysts.

Overall, we conclude that the cyst transport by currents can have an important effect on the sedimentary dinocyst assemblage composition as a paleoceanographic proxy. If a cyst is found outside of its expected habitat region, information on the particle transport could suggest whether a cyst actually occurs here (but perhaps in lower abundance) or whether the cyst was transported to the sediment sample locations. We recommend five factors to consider when relating micropaleontological data to the overlying surface water conditions: (1) What was the water depth? (2) Did the microplankton sink through aggregate formation? (3) Was the site under influence of strong ocean currents? (4) What was the orientation of this current? (5) Did strong gradients of environmental variables exist near the site? We further recommend for any microplankton-related data set to take particle transport into account when relating sedimentary data to oceanography. The particle tracking method provides an opportunity to quantify the probability that these factors matter at a specific sample location.

In general, the inferred PDFs after the backtracking of particles converged sufficiently fast to one shape and comprised multiple seasonal cycles. However, the low abundances of species in surface sediment samples could be related to rare events. Examples of rare events are polynya events (Holland, 2001), marine heatwaves, or severe storms (Ummenhofer & Meehl, 2017). Future simulations should run sufficiently long to include strong El Niño and La Niña events, which could influence the results. Such variability is averaged

out in the surface sediment samples but is currently not covered in the model runs. However, the rare occurrences have quite profound effects on modern analogue techniques, and therefore, it is important that we understand how these arrive at the sample site and what their ecological implications are.

We use the tails of the APDF as a measure of AB in this paper. However, different measures of AB could be applied in future research. It is intuitive to think about the differences of the PDF's higher-order modes such as the mean or standard deviation, although both are not informative with non-Gaussian PDFs. Furthermore, one could apply a measure which combines differences between the LPDF and the APDF in terms of all their modes (such as the Wasserstein distance; Ramdas et al., 2017). Then one can investigate whether the APDF is different from the LPDF, but on the other hand, it is not clear which mode(s) cause these differences.

No observed data of dinocysts close to the surface exists in the open ocean. Hence, we cannot compare our model results of lateral transports with measured data. Dinoflagellate data at the surface do exist (e.g., Eynaud et al., 1999) and in broad lines these do seem to confirm the overall sedimentary dinocyst biogeography, but it is not sufficiently known which cyst type the dinoflagellates form. Hence, we are limited to the sedimentary dinocyst assemblages.

Similar backtracking methods could be applied to other sinking proxies, such as planktic foraminifera (van Sebille et al., 2015) and coccoliths. However, it is important to take into account different properties of the proxy. For example, dinocysts relate directly to the environment at the surface, while another proxy can be influenced by the environment along a trajectory before sinking, or the productivity of other proxies in the water column could be different. Moreover, the sinking velocity of another proxy could be different compared to the sinking velocity of dinocysts. Hence, each microplankton group requires a specific type of modeling and inclusion of specific boundary conditions.

The results in this paper challenge the conventional transfer function methods. Future work is required to investigate whether a new type of transfer function, which corrects for lateral transport, could improve the skill of quantitative paleoceanographic reconstructions.

Acknowledgments
The code used for this work is distributed under the MIT license and can be found at the website (https://github.com/pdnooteboom/PO-dinocysts). This work was funded by the Netherlands Organization for Scientific Research (NWO), Earth and Life Sciences, through project ALWOP.207. The use of the SURFsara computing facilities was sponsored by NWO-EW (Netherlands Organisation for Scientific Research, Exact Sciences) under the project 15508. A. v. d. H. acknowledges travel support to network partners from the EPSRC-funded Past Earth Network (Grant EP/M008363/1). P. K. B. acknowledges funding through European Research Council Starting Grant 802835, OceaNice.

References

Alldredge, A. L., Passow, U., & Haddock, S. H. D. (1998). The characteristics and transparent exopolymer particle (TEP) content of marine snow formed from thecatedinoflagellates. *Journal of Plankton Research*, *20*(3), 393–406.

Anderson, D. M., Lively, J. J., Reardon, E. M., & Price, C. a. (1985). Sinking characteristics of dinoflagellate cysts. *Limnology and Oceanography*, *30*(5), 1000–1009. https://doi.org/10.4319/lo.1985.30.5.1000

Aumont, O., Ethé, C., Tagliabue, A., Bopp, L., & Gehlen, M. (2015). PISCES-v2: An ocean biogeochemical model for carbon and ecosystem studies. *Geoscientific Model Development*, *8*(8), 2465–2513. https://doi.org/10.5194/gmd-8-2465-2015

Azetsu-Scott, K., & Passow, U. (2004). Ascending marine particles: Significance of transparent exopolymer particles (TEP) in the upper ocean. *Limnology and Oceanography*, *49*(3), 741–748.

Bach, L. T., Boxhammer, T., Larsen, A., Hildebrandt, N., Schulz, K. G., & Riebesell, U. (2016). Influence of plankton community structure on the sinking velocity of marine aggregates. *Global Biogeochemical Cycles*, *30*, 1145–1165. https://doi.org/10.1002/2016GB005372

Berelson, W. M. (2002). Particle settling rates increase with depth in the ocean. *Deep Research Part II*, *49*, 237–251.

Bijl, P. K., Bendle, J. A. P., Bohaty, S. M., Pross, J., Schouten, S., Tauxe, L., et al. (2013). Eocene cooling linked to early flow across the Tasmanian Gateway. *Proceedings of the National Academy of Sciences*, *110*(24), 9645–9650. https://doi.org/10.1073/pnas.1220872110

Bijl, P. K., Houben, A. J., Hartman, J. D., Pross, J., Salabarnada, A., Escutia, C., & Sangiorgi, F. (2018). Paleoceanography and ice sheet variability offshore Wilkes Land, Antarctica - Part 2: Insights from Oligocene-Miocene dinoflagellate cyst assemblages. *Climate of the Past*, *14*(7), 1015–1033. https://doi.org/10.5194/cp-14-1015-2018

Bijl, P. K., Pross, J., Warnaar, J., Stickley, C. E., Huber, M., Guerstein, R., et al. (2011). Environmental forcings of Paleogene Southern Ocean dinoflagellate biogeography. *Paleoceanography*, *26*, PA1202. https://doi.org/10.1029/2009PA001905

Bringué, M., Pospelova, V., Tappa, E. J., & Thunell, R. C. (2019). Progress in oceanography dinoflagellate cyst production in the Cariaco Basin: A 12.5 year-long sediment trap study. *Progress in Oceanography*, *171*, 175–211. https://doi.org/10.1016/j.pocean.2018.12.007

Bringué, M., Thunell, R. C., Pospelova, V., Pinckney, J. L., Romero, O. E., & Tappa, E. J. (2018). Physico-chemical and biological factors influencing dinoflagellate cyst production in the Cariaco Basin. *Biogeosciences*, *15*, 2325–2348.

Chen, M., Ma, Q., Guo, L., Qiu, Y., Li, Y., & Yang, W. (2012). Deep-Sea Research II Importance of lateral transport processes to Chukchi Sea during summer 2003. *Deep Research Part II*, *81-84*, 53–62. https://doi.org/10.1016/j.dsr2.2012.03.011

Chi, L., Wolfe, C. L. P., & Hameed, S. (2018). Intercomparison of the Gulf Stream in ocean reanalyses : 1993–2010. *Ocean Modelling*, *125*, 1–21. https://doi.org/10.1016/j.ocemod.2018.02.008

Cramwinckel, M. J., van der Ploeg, R., Bijl, P. K., Peterse, F., Bohaty, S. M., Röhl, U., et al. (2019). Harmful algae and export production collapse in the equatorial Atlantic during the zenith of Middle Eocene Climatic Optimum warmth. *Geology*, *47*, 247–250.

Crouch, E. M., Mildenhall, D. C., & Neil, H. L. (2010). Distribution of organic-walled marine and terrestrial palynomorphs in surface sediments, offshore eastern New Zealand. *Marine Geology*, *270*(1-4), 235–256. https://doi.org/10.1016/j.margeo.2009.11.004

Crouch, E. M., Willumsen, P. S., Kulhanek, D. K., & Gibbs, S. J. (2014). A revised Paleocene (Teurian) dinoflagellate cyst zonation from eastern New Zealand. *Review of Palaeobotany and Palynology*, *202*, 47–79. https://doi.org/10.1016/j.revpalbo.2013.12.004

Dale, B. (1976). Cyst formation, sedimentation, and preservation: Factors affecting dinoflagellate assemblages in recent sediments from trondheimsfjord, Norway. *Review of Palaeobotany and Palynology*, *22*(1), 39–60. https://doi.org/10.1016/0034-6667(76)90010-5

Dale (1996). *Palynology principles and applications* (Chap. 31, pp. 1249–1275). Dallas, TX

Dale, B., Dale, A. L., & Jansen, J. H. F. (2002). Dinoflagellate cysts as environmental indicators in surface sediments from the Congo deep-sea fan and adjacent regions. *Palaeoecology*, *182*, 309–338. https://doi.org/10.1016/S0031-0182(02)00380-2

Datema, M., Sangiorgi, F., de Vernal, A., Reichart, G. J., Lourens, L. J., & Sluijs, A. (2017). Comparison of qualitative and quantitative dinoflagellate cyst approaches in reconstructing glacial-interglacial climate variability at West Iberian Margin IODP 'shackleton' Site U1385. *Marine Micropaleontology*, *136*, 14–29. https://doi.org/10.1016/j.marmicro.2017.08.003

de Schepper, S., Fischer, E. I., Groeneveld, J., Head, M. J., & Matthiessen, J. (2011). Deciphering the palaeoecology of Late Pliocene and Early Pleistocene dinoflagellate cysts. *Palaeogeography, Palaeoclimatology, Palaeoecology*, *309*(1–2), 17–32. https://doi.org/10.1016/j.palaeo.2011.04.020

de Vernal, A., Londeix, L., Mudie, P. J., Harland, R., Morzadec-Kerfourn, T. M. T., & Wrenn, J. J.-L. (1992). Quaternary organic-walled dinoflagellate cysts of the North Atlantic Ocean and adjacent seas: Ecostratigraphy and biostratigraphy, *Neogene Quat. Dinoflag. cysts acritarchs* (pp. 289–328). Dallas.

Delandmeter, P., & van Sebille, E. (2019). The Parcels v2.0 Lagrangian framework: New field interpolation schemes. *Geoscientific Model Development*. https://doi.org/10.5194/gmd-2018-339

Evitt, W. R. (1985). *Sporopollenin dinoflagellate cysts. Their morphology and interpretation* (pp. 333). Dallas: American Association of Stratigrafic Palynologists Foundation.

Eynaud, F., Giraudeau, J., Pichon, J. J., & Pudsey, C. J. (1999). Sea-surface distribution of coccolithophores, diatoms, silicoflagellates and dinoflagellates in the South Atlantic Ocean during the late austral summer 1995. *Deep Research*, *46*, 451–482.

Fahl, K., & Nöthing, E.-m. (2007). Lithogenic and biogenic particle fluxes on the Lomonosov Ridge (Central Arctic Ocean) and their relevance for sediment accumulation: Vertical vs. lateral transport. *Deep Research Part*, *1*(54), 1256–1272. https://doi.org/10.1016/j.dsr.2007.04.014

Fraser, C. I., Morrison, A. K., Hogg, A. M., Macaya, E. C., Sebille, E. V., Ryan, P. G., et al. (2018). Antarctica's ecological isolation will be broken by storm-driven dispersal and warming. *Nature Climate Change*, *8*, 704–708. https://doi.org/10.1038/s41558-018-0209-7

Frieling, J., & Sluijs, A. (2018). Towards quantitative environmental reconstructions from ancient non-analogue microfossil assemblages: Ecological preferences of Paleocene-Eocene dinoflagellates. *Earth-Science Reviews*, *185*, 956–973. https://doi.org/10.1016/j.earscirev.2018.08.014

Harland, R., & Pudsey, C. J. (1999). Dinoflagellate cysts from sediment traps deployed in the Bellingshausen, Weddell and Scotia seas, Antarctica. *Marine Micropaleontology*, *37*, 77–99.

Hartman, J. D., Bijl, P. K., & Sangiorgi, F. (2018). A review of the ecological affinities of marine organic microfossils from a Holocene record offshore of Adelie Land (East Antarctica). *Journal of Micropalaeontology*, *37*(2), 445–497. https://doi.org/10.5194/jm-37-445-2018

Hecht, M. W., & Smith, R. D. (2013). A review of North Atlantic Ocean Modeling in an eddying regime. *Geophysical Monograph Series*, *177*, 108–109. https://doi.org/10.1029/177GM15

Holland, D. (2001). Explaining the Weddell Polynya a large ocean eddy shed at Maud Rise. *Science*, *292*, 1697–1701.

Honjo, S., Spencer, D. W., & Farrington, J. W. (1982). Deep advective transport of lithogenic particles in Panama Basin. *Science*, *216*, 516–518.

Houben, A. J., Bijl, P. K., Pross, J., Bohaty, S. M., Passchier, S., Stickley, C. E., et al. (2013). Reorganization of Southern Ocean plankton ecosystem at the onset of Antarctic glaciation. *Science*, *340*, 341–344. https://doi.org/10.1126/science.1223646

Jokulsdottir, T., & Archer, D. (2016). A stochastic, Lagrangian model of sinking biogenic aggregates in the ocean (SLAMS 1.0): Model formulation, validation and sensitivity. *Geoscientific Model Development*, *9*(4), 1455–1476. https://doi.org/10.5194/gmd-9-1455-2016

Lange, M., & Sebille, E. V. (2017). Parcels v0.9: Prototyping a Lagrangian ocean analysis framework for the petascale age. *Geoscientific Model Development*, *10*(11), 4175–4186. https://doi.org/10.5194/gmd-10-4175-2017

Madec, G. (2016). NEMO ocean engine, 27.

Marret, F., De Vernal, A., Benderra, F., & Harland, R. (2001). Late quaternary sea-surface conditions at DSDP Hole 594 in the Southwest Pacific Ocean based on dinoflagellate cyst assemblages. *Journal of Quaternary Science*, *16*(7), 739–751. https://doi.org/10.1002/jqs.648

Marshall, J., & Radko, T. (2003). Residual-mean solutions for the Antarctic Circumpolar Current and its associated overturning circulation. *Journal of Physical Oceanography*, *33*(11), 2341–2354. https://doi.org/10.1175/1520-0485(2003)033<2341:RSFTAC>2.0.CO;2

Marzocchi, A., Hirschi, J. J., Holliday, N. P., Cunningham, S. A., Blaker, A. T., & Coward, A. C. (2015). The North Atlantic subpolar circulation in an eddy-resolving global ocean model. *Journal of Marine Systems*, *142*, 126–143. https://doi.org/10.1016/j.jmarsys.2014.10.007

Masumoto, Y. (2010). Sharing the results of a high-resolution ocean general circulation model under a multi-discipline framework—A review of OFES activities. *Ocean Dynamics*, *60*, 633–652. https://doi.org/10.1007/s10236-010-0297-z

Masumoto, Y., Sasaki, H., Kagimoto, T., Komori, N., Ishida, A., Sasai, Y., et al. (2004). A fifty-year eddy-resolving simulation of the world ocean—Preliminary outcomes of OFES (OGCM for the Earth simulator). *Journal of the Earth Simulator*, *1*, 35–56.

Matano, R. P., Palma, E. D., & Piola, A. R. (2010). The influence of the Brazil and Malvinas Currents on the Southwestern Atlantic Shelf circulation. *Ocean Science*, *6*(4), 983–995. https://doi.org/10.5194/os-6-983-2010

Matthiessen, J. (1997). Organic-walled dinoflagellate cysts: Palynologycal tracers of sea-surface conditions in middle to high latitude marine environments. *Geobios*, *30*(7), 905–920.

McWilliams, J. C., Liu, Y., Dong, C., & Chen, D. (2014). Global heat and salt transports by eddy movement. *Nature Communications*, *5*, 1–6. https://doi.org/10.1038/ncomms4294

Monroy, P., Hernández-García, E., Rossi, V., & López, C. (2017). Modeling the dynamical sinking of biogenic particles in oceanic flow. *Nonlinear Processes in Geophysics*, *24*(2), 293–305.

Montresor, M., Nuzzo, L., & Mazzocchi, M. G. (2003). Viability of dinoflagellate cysts after the passage through the copepod gut. *Journal of Experimental Marine Biology and Ecology*, *287*(2), 209–221. https://doi.org/10.1016/S0022-0981(02)00549-X

Mudie, P. (1996). Pellets of dinoflagellate-eating zooplankton, (June), 1087–1089.

Ohlwein, C., & Wahl, E. R. (2012). Review of probabilistic pollen-climate transfer methods. *Quaternary Science Reviews*, *31*, 17–29. https://doi.org/10.1016/j.quascirev.2011.11.002

Orsi, A. H., Whitworth, T., & Nowlin, W. D. Jr (1995). On the meridional extent and fronts of the Antarctic Circumpolar Current. *Deep Research*, *42*(5), 641–673.

Pospelova, V., Zonneveld, K. A. F., Heikkilä, M., Bringué, M., Price, A. M., Esenkulova, S., et al. (2018). Seasonal, annual, and inter-annual Spiniferites cyst production: A review of sediment trap studies. *Palynology*, *42*(S1), 162–181. https://doi.org/10.1080/01916122.2018.1465738

Prebble, J. G., Crouch, E. M., Carter, L., Cortese, G., Bostock, H., & Neil, H. (2013). An expanded modern dinoflagellate cyst dataset for the Southwest Pacific and Southern Hemisphere with environmental associations. *Marine Micropaleontology*, *101*, 33–48. https://doi.org/10.1016/j.marmicro.2013.04.004

Qin, X., van Sebille, E., & Sen Gupta, A. (2014). Quantification of errors induced by temporal resolution on Lagrangian particles in an eddy-resolving model. *Ocean Modelling*, *76*, 20–30. https://doi.org/10.1016/j.ocemod.2014.02.002

Ramdas, A., Trillos, N. G., & Cuturi, M. (2017). On Wasserstein two-sample testing and related families of nonparametric tests. *Entropy*, *19*(47), 1–15. https://doi.org/10.3390/e19020047

Riley, J. S., Sanders, R., Marsay, C., Moigne, F. A. C. L., Achterberg, E. P., & Poulton, A. J. (2012). The relative contribution of fast and slow sinking particles to ocean carbon export. *Global Biogeochemical Cycles*, *26*, GB1026. https://doi.org/10.1029/2011GB004085

Rixen, T., Gaye, B., Emeis, K.-c., & Ramaswamy, V. (2019). The ballast effect of lithogenic matter and its influences on the carbon fluxes in the Indian Ocean. *Biogeosciences*, *16*, 485–503.

Sasaki, H., Nonaka, M., Masumoto, Y., Sasai, Y., Uehara, H., & Sakuma, H. (2008). chap An eddy-resolving hindcast simulation of the quasiglobal ocean from 1950 to 2003 on the Earth simulator. In K. Hamilton, & W. Ohfuchi (Eds.), *High resolution numerical modelling of the atmosphere and ocean* (Vol. 10, pp. 157–185). New York: Springer.

Schmeits, M. J., & Dijkstra, H. A. (2001). Bimodal behavior of the Kuroshio and the Gulf Stream. *Journal of Physical Oceanography*, *31*(12), 3435–3456.

Schmidt, K., Rocha, C. L. D. L., Gallinari, M., & Cortese, G. (2014). Not all calcite ballast is created equal: Differing effects of foraminiferan and coccolith calcite on the formation and sinking of aggregates. *Biogeosciences*, *11*, 135–145. https://doi.org/10.5194/bg-11-135-2014

Sluijs, A., Pross, J., & Brinkhuis, H. (2005). From greenhouse to icehouse; organic-walled dinoflagellate cysts as paleoenvironmental indicators in the Paleogene. *Earth-Science Reviews*, *68*(3-4), 281–315. https://doi.org/10.1016/j.earscirev.2004.06.001

Sluijs, A., Schouten, S., Pagani, M., Woltering, M., Brinkhuis, H., Damsté, J. S., et al. (2006). Subtropical Arctic Ocean temperatures during the Palaeocene/Eocene thermal maximum. *Nature*, *441*(7093), 610–613. https://doi.org/10.1038/nature04668

Smayda, T. J. (2002). Turbulence, watermass stratification and harmful algal blooms: An alternative view and frontal zones as 'pelagic seed banks'. *Harmful Algae*, *1*, 95–112.

Storkey, D., Blockley, E. W., Furner, R., Guiavarc, C., Lea, D., Martin, M. J., et al. (2014). Forecasting the ocean state using NEMO: The new FOAM system. *Journal of Operational Oceanography*, *3*(1), 3–15. https://doi.org/10.1080/1755876X.2010.11020109

Tang, Y., Lemaitre, N., Castrillejo, M., Masqué, P., & Stewart, G. (2019). Po/^{210}Pb disequilibria along the North Atlantic GEOTRACES GA01 transect: GEOVIDE cruise. *Biogeosciences*, *16*, 309–327.

Telford, R. J., & Birks, H. J. B. (2009). Evaluation of transfer functions in spatially structured environments. *Quaternary Science Reviews*, *28*(13–14), 1309–1316. https://doi.org/10.1016/j.quascirev.2008.12.020

Tournadre, J., Girard-ardhuin, F., & Legrésy, B. (2012). Antarctic icebergs distributions, 2002–2010. *Journal of Geophysical Research*, *117*, C05004. https://doi.org/10.1029/2011JC007441

Ummenhofer, C. C., & Meehl, G. A. (2017). Extreme weather and climate events with ecological relevance: A review. *Philosophical Transactions of the Royal Society B*, *372*, 20160135.

Uotila, P., Iovino, D., Vancoppenolle, M., Lensu, M., Rousset, C., Universités, S., et al. (2017). Comparing sea ice, hydrography and circulation. *Geoscientific Model Development*, *10*, 1009–1031. https://doi.org/10.5194/gmd-10-1009-2017

van Sebille, E., Griffies, S. M., Abernathey, R., Adams, T. P., Berloff, P., Biastoch, A., et al. (2018). Lagrangian ocean analysis: Fundamentals and practices. *Ocean Modelling*, *121*, 49–75. https://doi.org/10.1016/j.ocemod.2017.11.008

van Sebille, E., Scussolini, P., Durgadoo, J. V., Peeters, F. J. C., Biastoch, A., Weijer, W., et al. (2015). Ocean currents generate large footprints in marine palaeoclimate proxies. *Nature Communications*, *6*, 6521. https://doi.org/10.1038/ncomms7521

Volkov, D. L., Lee, T., & Fu, L. L. (2008). Eddy-induced meridional heat transport in the ocean. *Geophysical Research Letters*, *35*, L20601. https://doi.org/10.1029/2008GL035490

Yool, A., Popova, E. E., & Anderson, T. R. (2013). MEDUSA-2.0: An intermediate complexity biogeochemical model of the marine carbon cycle for climate change and ocean acidification studies. *Geoscientific Model Development*, *6*(5), 1767–1811. https://doi.org/10.5194/gmd-6-1767-2013

Zonneveld, K., Marret, F., Versteegh, G., Bogus, K., Bonnet, S., Bouimetarhan, I., et al. (2013a). Geographic distribution of dinoflagellate cysts in surface sediments. PANGAEA, https://doi.org/10.1594/PANGAEA.818280

Zonneveld, K. A., Marret, F., Versteegh, G. J., Bogus, K., Bonnet, S., Bouimetarhan, I., et al. (2013b). Atlas of modern dinoflagellate cyst distribution based on 2405 data points. *Review of Palaeobotany and Palynology*, *191*, 1–197. https://doi.org/10.1016/j.revpalbo.2012.08.003